Journal of Power Sources 270 (2014) 1–8

Contents lists available at ScienceDirect

Journal of Power Sources

journal homepage: www.elsevier.com/locate/jpowsour

Sulfur nanocrystals anchored graphene composite with highly improved electrochemical performance for lithium–sulfur batteries

Jun Zhang [a, *], Zimin Dong [a], Xiuli Wang [b], Xuyang Zhao [b], Jiangping Tu [b], Qingmei Su [a], Gaohui Du [a, *]

[a] Key Laboratory of the Ministry of Education for Advanced Catalysis Materials, Institute of Physical Chemistry, Zhejiang Normal University, Jinhua 321004, China

[b] Key Laboratory of Advanced Materials and Applications for Batteries of Zhejiang Province, Department of Materials Science and Engineering, Zhejiang University, Hangzhou 310027, China

HIGHLIGHTS

- A one-pot hydrothermal method to prepare NanoS@graphene composite.
- It showed highly improved electrochemical performance for Li–S battery.
- XPS revealed strong bonding between sulfur and graphene.
- The strong bonding immobilized sulfur and polysulfides species.
- Higher utilization of sulfur and better capacity retention were obtained.

GRAPHICAL ABSTRACT

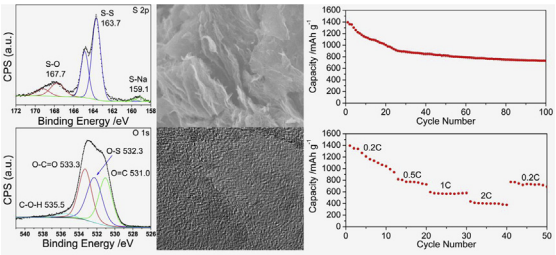

Sulfur nanocrystals anchored graphene for Li–S battery

ARTICLE INFO

Article history:
Received 16 June 2014
Received in revised form
13 July 2014
Accepted 15 July 2014
Available online 23 July 2014

Keywords:
Lithium–sulfur batteries
Sulfur–graphene composites
Sulfur nanocrystals
Electrochemical performance
X-ray photoelectron spectra

ABSTRACT

Two kinds of graphene–sulfur composites with 50 wt% of sulfur are prepared using hydrothermal method and thermal mixing, respectively. Transmission Electron Microscopy (TEM) and Energy Dispersive X-ray Spectra mapping show that sulfur nanocrystals with size of ~5 nm dispersed on graphene sheets homogeneously for the sample prepared by hydrothermal method (NanoS@G). While for the thermal mixed graphene–sulfur composite (S–G mixture), sulfur shows larger and uneven size (50–200 nm). X-ray Photoelectron Spectra (XPS) reveals the strong chemical bonding between the sulfur nanocrystals and graphene. Comparing with the S–G mixture, the NanoS@G composite shows highly improved electrochemical performance as cathode for lithium–sulfur (Li–S) battery. The NanoS@G composite delivers an initial capacity of 1400 mAh g^{-1} with the sulfur utilization of 83.7% at a current density of 335 mA g^{-1}. The capacity keeps above 720 mAh g^{-1} over 100 cycles. The strong adherence of the sulfur nanocrystals on graphene immobilizes sulfur and polysulfides species and suppressed the "shuttle effect", resulting higher coulombic efficiency and better capacity retention. Electrochemical impedance also suggests that the strong bonding enabled rapid electronic/ionic transport and improved electrochemical kinetics, therefore good rate capability is obtained. These results demonstrate that the NanoS@G composite is a very promising candidate for high-performance Li–S batteries.

1. Introduction

With the high theoretical specific capacity (1675 mAh g^{-1}) based on the electrochemical redox reaction $16Li + S_8 \leftrightarrow 8Li_2S$, elemental sulfur has been considered to be one of most promising

* Corresponding authors. Tel.: +86 182 6704 9959; fax: +86 579 8228 2234.
E-mail addresses: zhangjun@zjnu.cn, zhangjun1985@gmail.com (J. Zhang), gaohuidu@zjnu.edu.cn (G. Du).

http://dx.doi.org/10.1016/j.jpowsour.2014.07.089
0378-7753/

alternatives to replace the intercalation cathode materials for secondary lithium batteries [1]. Lithium–sulfur (Li–S) batteries also possess a wide operating temperature range, and the intrinsic protection mechanism from overcharging, which enhances battery safety [2]. In addition, sulfur is environmentally friendly, abundant on earth and inexpensive. With these excellences, Li–S battery systems are considered to be the candidate next-generation power source for electric and hybrid electric vehicles.

Despite the considerable advantages of Li–S battery, it faces serious challenges [3]. The inherent poor electrical conductivity of sulfur (5×10^{-30} S cm^{-1} at room temperature), shuttling of soluble polysulfides to anode and reacting with metallic lithium during charging, and agglomeration of insulating Li_2S_2/Li_2S on the cathode during discharge, result in decreased utilization of active material, reduced coulombic efficiency, and severe capacity fading of the battery.

Electrolyte additives such as $LiNO_3$ are used to form a passive layer on the surface of metallic lithium anode preventing further reaction with polysulfides, and the coulombic efficiency is improved to a satisfied level [4,5]. On the other hand, extensive research working on the improvement of the electric conductivity of sulfur based cathode achieves great success. Among the supporting matrix for sulfur, carbon based materials and conductive polymers are the main choices. Conductive matrix such as carbon nanotubes (CNTs) [6], mesoporous carbon [7,8], graphene [9–13], polyaniline [14,15], polypyrrole [16,17], etc, work both as the reservoir to accommodate sulfur and the adsorbent to suppress the loss of polysulfide intermediates. Graphene, as an emerging nanomaterial that composed of two-dimensional graphite layers with one-atom-thick sheet of sp^2 bonded carbon atoms, exhibits superior electron mobility, extremely high specific surface area, and good chemical tolerance, enabling it to be preferred candidate for energy storage applications. Several groups have demonstrated that graphene (or graphene oxide) is an outstanding support for sulfur [9–13]. Though with improved electrochemical performance, the interactions between sulfur and graphene is very weak due to the synthesis process, mostly in two approaches, thermal mixing and chemical reaction deposition, both of which only enable physical absorption, resulting in unsatisfied long-term stability and rate capability.

Several pioneering works have proposed that to enhance interaction between conductive matrix and sulfur or polysulfides is an effective approach to lock the active materials. Y.G. Zhang's group [18] deposited a thin and uniform sulfur coating on graphene oxide which acts as the sulfur immobilizer, and demonstrated that a high reversible capacity up to 950 mAh g^{-1} after 50 cycles was obtained due to the strong interaction between graphene oxide and sulfur or polysulfides. It has also been found by A.S. Yu et al. [19] that surface functionalized graphene with strong interaction with sulfur and polysulfides makes great improvement on reversible capacity. However, it is a challenge to develop a simple method to synthesize graphene/sulfur composites with strong adherence between graphene and sulfur. It also remains unknown that the influence of sulfur's morphology on its electrochemical performance.

Herein, we report a one-pot method to prepare sulfur nanocrystals anchored graphene composite (NanoS@G). Comparing with thermal mixing graphene/sulfur composite (S–G mixture), highly improved electrochemical performance was obtained for Li–S cell with NanoS@G as the cathode. Chemical bonding evidence and electrochemical impedance was investigated to understand the mechanisms.

2. Experimental

2.1. Synthesis of NanoS@G

The graphene oxide (GO) was made by a modified Hummers method. Firstly, 300 mg GO was dispersed in 100 mL 0.1% sodium

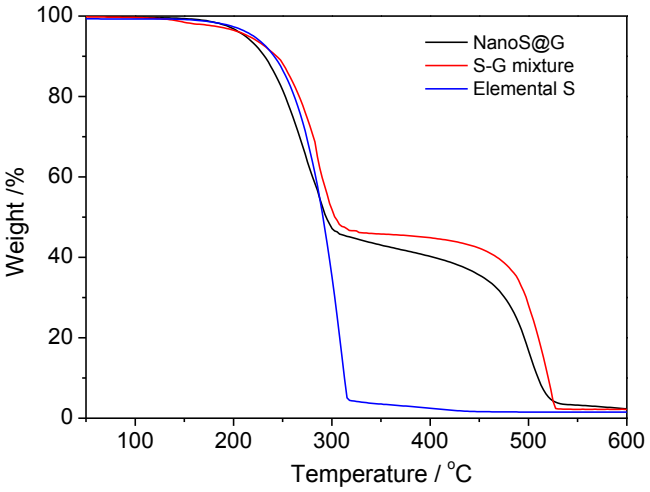

Fig. 1. TG curves of elemental sulfur, the NanoS@G composite and the S–G mixture.

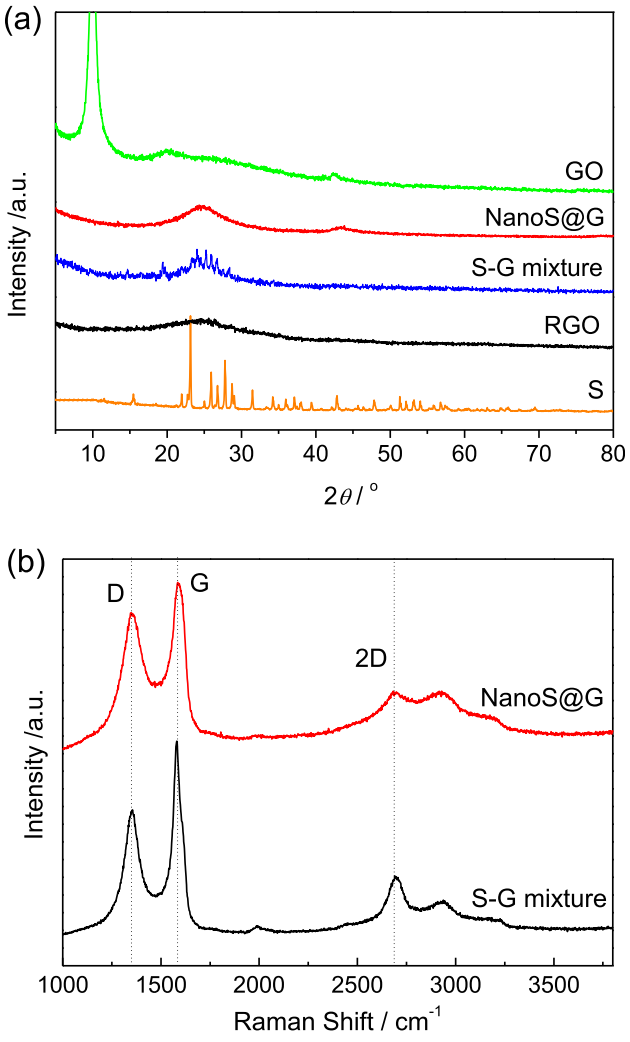

Fig. 2. (a) XRD patterns of elemental sulfur, graphene oxide, reduced graphene, the NanoS@G composite and the S–G mixture; (b) the Raman spectra of the NanoS@G composite and the S–G mixture.

dodecylsulphate aqueous solution. 300 mg sulfur nanoparticles with average diameter of 50 nm (received from Beijing DK Nano technology Co., LTD) was dispersed in 100 mL distilled water in an ultrasonic bath. The two kinds of aqueous solutions, were mixed and ultrasonicated for 30 min, transferred into Teflon-lined stainless steel autoclave tightly sealed and heated at a temperature of 160 °C in a preheated electric oven for 12 h. After the reaction was complete, the autoclave was allowed to cool to room temperature and the precipitates were centrifuged and washed thoroughly with water and ethanol. The product was dried at 60 °C overnight. A sulfur–graphene mixture (S–G mixture) was prepared for comparison. Sulfur and reduced graphene oxide (RGO) were mixed through grinding, and heated for 12 h at 160 °C. RGO was prepared by expanding GO at 200 °C following reducing it at 450 °C for 2 h.

2.2. Material characterization

Powder X-ray diffraction (XRD, CuKα radiation, Philips PW3040/60) was used to verify the component of the composite. The sulfur content in the G/S was ascertained by the thermogravimetric/differential thermal analysis (TG/DTA) measurement (Netzsch STA 449C thermal analyzer). The morphologies were examined by scanning electron microscopy (SEM, Hitachi S-4800), and transmission electron microscopy (TEM, JEM 2010F). X-ray photoelectron spectra (XPS) were performed on an ESCALAB 250Xi Spectrometer (Thermo Scientific). Raman spectra were recorded on a Renishaw RM1000 confocal microprobe Raman system using an excitation laser of 514.5 nm, in a range of 100–4000 cm^{-1}.

2.3. Electrochemical measurement

The electrodes were prepared by dispersing the as-prepared composites (75 wt%), acetylene carbon black (15 wt%) and poly(-vinylidene fluoride) binder (10 wt%) in *N*-methyl-2-pyrrolidone solvent to form a slurry. The slurry was pasted onto Al foil current collector and dried at 60 °C for 12 h in a vacuum oven. The electrochemical measurements were carried out by two-electrode coin cells with a lithium foil as the counter electrode. The CR2025-type coin cells were assembled in an argon-filled glove box. The electrolyte solution was 1 M LiTFSI, 0.1 M $LiNO_3$ in a solvent of DOL:DME (1:1 in volume). Cyclic voltammetry (CV) and electrochemical impedance spectrometry were carried out on a CHI 604D electrochemistry workstation (Shanghai Chenhua Instruments Co. Ltd.). The galvanostatic charge and discharge measurements were conducted on an NEWARE battery test system at different current densities in the voltage range from 1.5 to 3.0 V.

3. Results and discussion

The sulfur content of the composites was determined using thermogravimetry. Fig. 1 shows that sulfur starts to evaporate at 200 °C and is evaporated completely up to 350 °C. The contents of sulfur in the two composites are both about 50%, as calculated from the curves. Fig. 2a shows the XRD patterns of the starting materials: sulfur, graphene oxide (GO), reduced graphene oxide (RGO) and the as-prepared composites NanoS@G and S–G mixture. Comparing with elemental sulfur, it can be seen in the NanoS@G composite that the characteristic peaks of sulfur become not distinct after the hydrothermal process. Only two broadened peaks centered at 24.5° and 43.5° are found, suggesting that the size of sulfur is very small or sulfur is amorphous. The broaden peak at 24.5° can also be attributed to graphene, meanwhile the characteristic peak at 10° corresponding to GO disappears, demonstrating that graphene oxide is reduced through the hydrothermal process. It is well known that GO can be hydrothermally reduced at high pressure as reported previously [20,21]. Besides, the S–G mixture still shows some characteristic peaks of orthorhombic S_{18} (JCPDS No. 72-0409), which is different with elemental sulfur (orthorhombic S_8, JCPDS: 85-0799). Apparently, sulfur changed its form during the synthesis. It's not very common for orthorhombic S_{18} phase at room temperature, which may due to the coexistence of graphene.

Fig. 2b shows the Raman spectra of NanoS@G and S–G mixture. The D band centered at 1350 cm^{-1} indicates the disordered arrangement of six-fold aromatic carbon ring, and the G band centered at 1580 cm^{-1} represents the sp^2-bonded carbon atoms of graphite layers. The 2D band at 2695 cm^{-1} which is caused from a

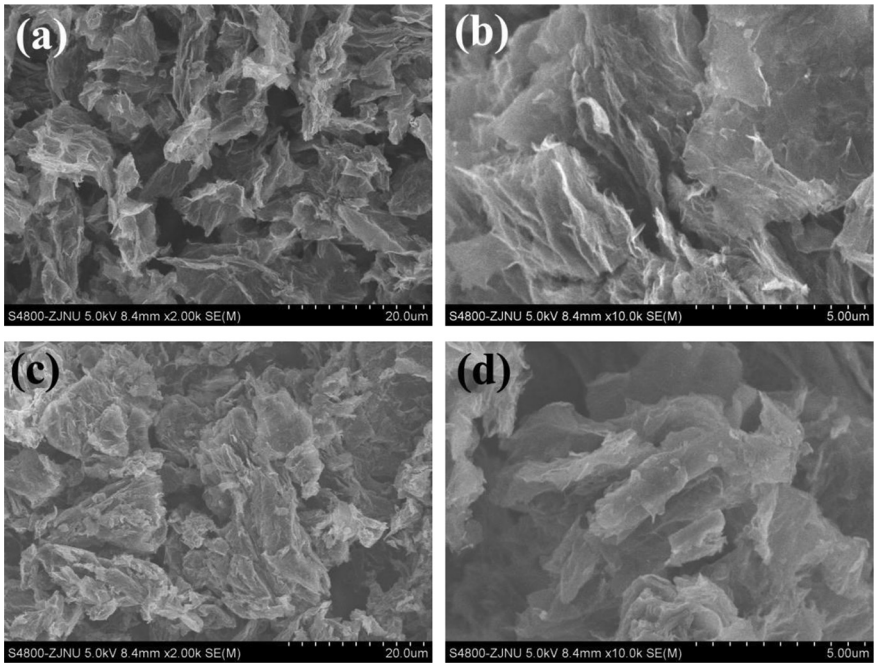

Fig. 3. SEM images of the NanoS@G composite (a, b) and the S–G mixture (c, d).

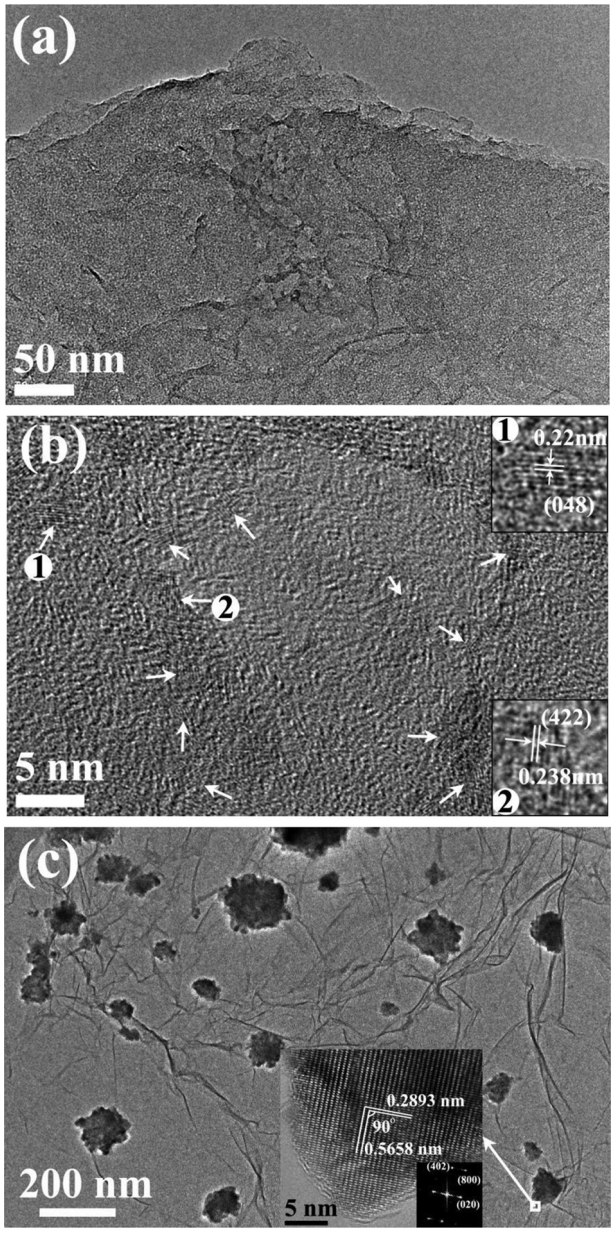

Fig. 4. TEM images of the NanoS@G composite (a, b) and the S–G mixture (c) (arrows denote the sulfur nanocrystals and insets are HRTEM images).

two-phonon resonant scattering process is the characteristic of ordered six-member ring of C atoms of graphene structure [22]. The ratio of D and G bands (I_D/I_G) is calculated to be 1.46 and 1.42 for RGO in NanoS@G and S–G mixture respectively, indicating that RGO in both samples have similar reduced level.

The SEM image of the NanoS@G composite shows that the graphene keeps porous and layered structure (Fig. 3a and b). In contrast, the S–G mixture exhibits a compact agglomeration morphology with some large sulfur particles (Fig. 3c and d). Fig. 4 shows the TEM images of the samples. Graphene sheets in both samples are thin and wrinkled. For the NanoS@G composite, very small size of sulfur nanocrystals can be found in high resolution TEM (Fig. 4b), which confirms the XRD result. Notably, the S–G mixture shows large sulfur particles with size of 50–200 nm distribute on graphene sheets. The well-resolved lattice fringes in the HRTEM image (inset) correspond to an interplanar spacing of 0.5658 nm and 0.2893 nm, consistent with the (020) planes and (402) planes of the orthorhombic sulfur respectively. The sulfur and carbon elemental maps (Fig. 5) of the NanoS@G composite confirm the homogeneous distribution of sulfur on the surface of graphene sheets.

To verify the interaction between sulfur and graphene, X-ray photoelectron spectroscopy (XPS) was employed on the two composites. Fig. 6a and b shows the high resolution core level spectra of S 2p in NanoS@G and S–G mixture. The peaks at 163.7 eV and 164.8 eV are attributed to S $2p_{3/2}$ and S $2p_{1/2}$, respectively [23]. The peak at 168.5 eV is assigned to S–O bond [24]. An additional peak at 159.3 eV in NanoS@G is attributed to the S–Na bond induced by the residual surfactant [24]. The content of S–O bond in NanoS@G (20.2%) is higher than that in S–G mixture (12.1%), indicating a much better bonding of sulfur and graphene via the hydrothermal process. This is further confirmed by the O 1s core level spectra shown in Fig. 6c and d, where the content of O–S bond centered at 532.15 eV [23] account for 33.6% area in NanoS@G *vs* 19% in S–G mixture. The C 1s core level spectra of both samples show characteristics of reduced graphene, except that the NanoS@G composite has a slightly higher content of C–O/C=O bonds, suggesting that hydrothermal reduction is not as complete as thermal reduction. Detailed fitting parameters are listed in Table 1. From the above analysis, it has been demonstrated that this one-pot hydrothermal method is an effective way to synthesize homogeneous sulfur anchoring graphene composite with strong interaction. And we expect that the strong adherence of sulfur on graphene through S–O bonding is favorable to restrain sulfur and polysulfides, improving the utilization of active materials and suppressing shuttle effect.

Fig. 7a shows the first three cyclic voltammograms (CV) of the cell with the NanoS@G composite as cathode material. The potential was swept from 1.5 to 3.0 V at a scan rate of 0.1 mV s^{-1}. Two cathodic peaks are observed at ~2.3 V and ~2.0 V, corresponding to the multiple reaction mechanism between sulfur and lithium that the reduction of S_8 to polysulphide (Li_2S_n, $2 < n < 8$), and further reduction to Li_2S_2/Li_2S, respectively. Polarization is observed in the first activation cycle with a peak shift from 2.32 to 2.25 V, which is attributed to overcoming the strong bonding energy with graphene [25,26]. In the anodic process, an oxidation peak at 2.4 V with a shoulder at 2.5 V corresponds to the reverse conversion of Li_2S_2/Li_2S to polysulfides and sulfur. These results are in consistent with galvanostatic discharge/charge profiles shown in Fig. 7b, that the charge/discharge plateaus exactly resemble the redox peaks observed in the CV scans.

Fig. 7c compares the cycling performance of NanoS@G composite and S–G mixture. A discharge capacity of 1400 mAh g^{-1} is obtained for the NanoS@G composite in the first discharge process, indicating a high utilization of sulfur (83.7%), which is much higher than that of the sulfur nanocrystal/fibrous graphene hybrid [23] and graphene-encapsulated sulfur particles [27,28], and comparable to sulfur/three-dimensional graphene/MWCNT composite and uniformly dispersed sulfur on reduced graphene oxide [25,26]. The discharge capacity of the NanoS@G composite can be maintained at ~720 mAh g^{-1} after 100 cycles, much higher than that of the S–G mixture [29]. Further comparison with various graphene/sulfur composites is listed in Table 2. The coulombic efficiency of the NanoS@G composite keeps steadily around 98% throughout the charge/discharge process, while the S–G mixture shows acute fluctuation coulombic efficiency from 93% to 109%, suggesting that the NanoS@G composite offers superior ability to suppress the shuttle effect.

Rate capability of the NanoS@G composite was examined by changing the charge/discharge current densities every 10 cycles. As shown in Fig. 7d, when the cell is charged and discharged at 0.2 C,

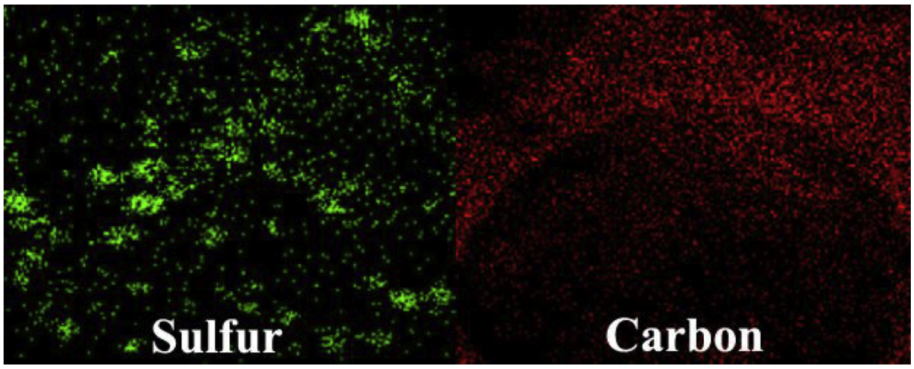

Fig. 5. Sulfur and carbon elemental mapping of the NanoS@G composite in the area of 1 μm × 0.8 μm.

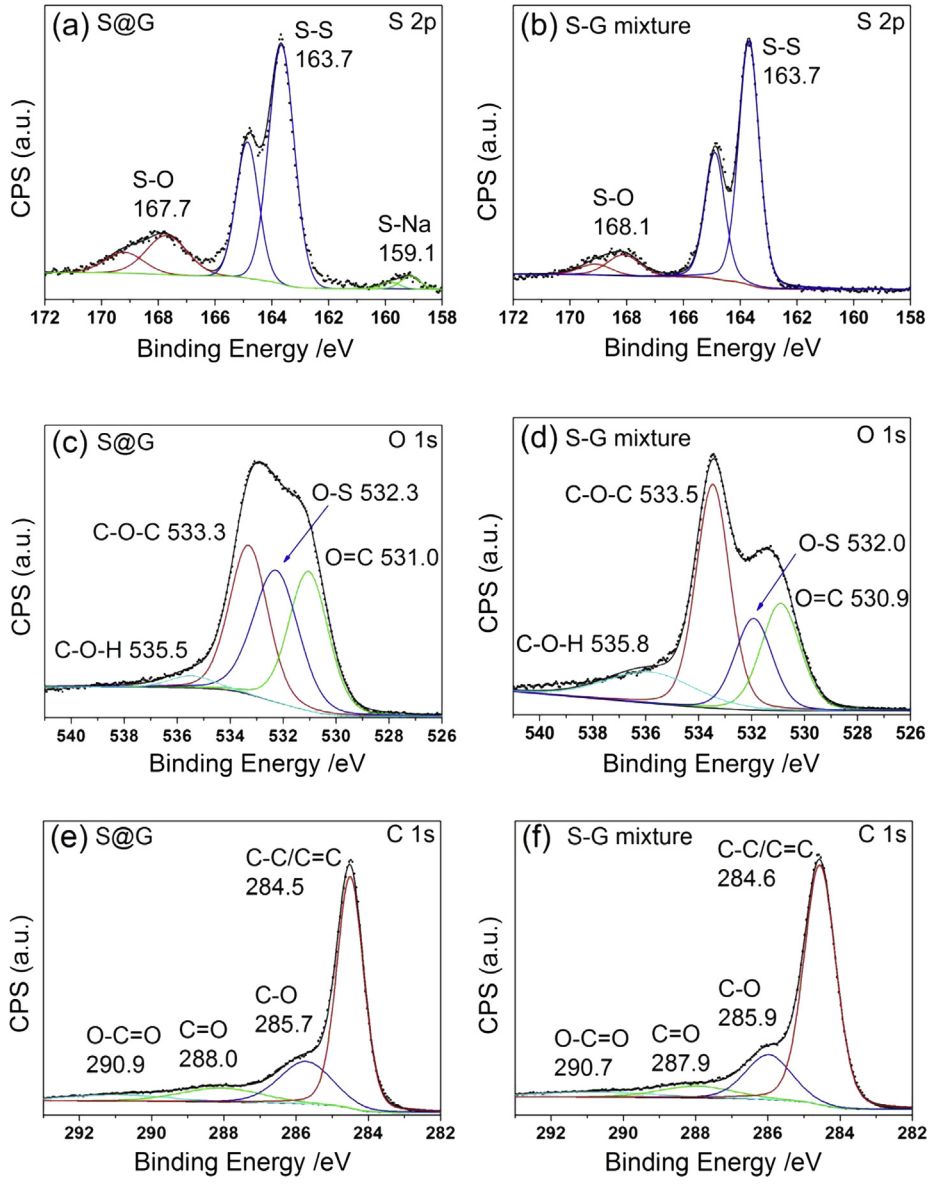

Fig. 6. S 2p, O 1s and C 1s core level spectra of the NanoS@G composite(a, c, e) and the S–G mixture (b, d, f), respectively.

Table 1
XPS fitting parameters.

		NanoS@G			S–G mixture		
		Peak position	FWHM	Area %	Peak position	FWHM	Area %
O 1s	C–O–H	535.5	2.0	3.1	535.8	4.0	15.7
	O–C=O	533.3	1.7	32.3	533.5	1.5	42.0
	O–S	532.3	2.0	33.6	532.0	1.7	19.0
	O=C	531.0	1.7	31.0	530.9	1.7	23.3
S 2p	S–O	167.7	1.7	20.2	168.1	1.4	12.1
	S–S	163.7	1.1	76.7	163.7	0.9	87.9
	S–Na	159.1	0.8	3.1	–	–	–
C 1s	O–C=O	290.9	3.2	5.9	290.7	3.9	5.3
	C=O	288.1	2.6	11.1	288.0	2.5	7.9
	C–O	285.7	1.7	22.1	285.9	1.5	18.5
	C–C/C=C	284.5	0.87	60.8	284.5	1.0	68.3

discharge capacity up to about 1400 mAh g^{-1} can be obtained. With the increase of current rate to 1C (1.67 A g^{-1}) and 2C (3.35 A g^{-1}), the NanoS@G composite delivers steady capacities up to ~570 mAh g^{-1} and 400 mAh g^{-1}, demonstrating a high rate capability. Moreover, a reversible capacity as high as 730 mAh g^{-1} can be recovered when the current was restored to 0.2 C.

The electrodes with NanoS@G and S–G mixture were further examined by the electrochemical impedance spectrometry (EIS), as shown in Fig. 8a. The measurements were taken at 2.5 V at the pristine state (before charge/discharge cycling) and the cycled state (after the cells were discharged/charged for 10 cycles), respectively. The spectra are fitted using an equivalent circuit shown in Fig. 8b. R_{el} and R_{sl}, and R_{ct} denote the resistances of the electrolyte, surface film (electrolyte–electrode interface), and charge transfer, respectively. The simulating parameters are listed in Table 3. The resistances of the electrolyte (R_{el}) in both cells are quite close, while this resistance increases slightly after charge/discharge cycle, which is ascribed to the dissolved polysulfides in the electrolyte that cause higher viscosity and lower lithium ion mobility. A higher increase of R_{el} is found in the cell with S–G mixture, indicating a higher concentration of the polysulfides is dissolved in the electrolyte. The increase of resistances related to surface film (R_{sl}) of both electrodes could be attributed to the deposition of inactive and insulating Li_2S_2/Li_2S on their surface during the charge/discharge cycle. Notably, the EIS reveals a much lower electrochemical impedance of resistances related to electrode/electrolyte interface and charge transfer of NanoS@G than those of S–G mixture. It is believed that the thin graphene and nanosized sulfur lead to short Li^+ diffusion distances, meanwhile the open porous structure provides rapid ion transport pathways [23]. Unique structure of the NanoS@G composite that sulfur nanoparticles anchor on highly conductive graphene sheets with strong bonding enables rapid electronic/ionic transport and improved electrochemical kinetics, resulting in both superior specific capacity and high rate capability.

4. Conclusions

In summary, we synthesized a sulfur anchored graphene composite via a one-pot hydrothermal method. Comparing with the thermal mixed samples of RGO and sulfur, the NanoS@G composite demonstrates significant enhancement of the electrochemical properties of cathode in Li–S batteries. TEM and EDX mapping showed that sulfur nanocrystals with size of ~5 nm dispersed on graphene sheets homogeneously for the sample prepared by hydrothermal method (NanoS@G). XPS revealed the strong chemical bonding between the sulfur nanocrystals and graphene. The strong adherence of the sulfur nanocrystals on graphene, which was induced by the hydrothermal treatment, immobilized sulfur and

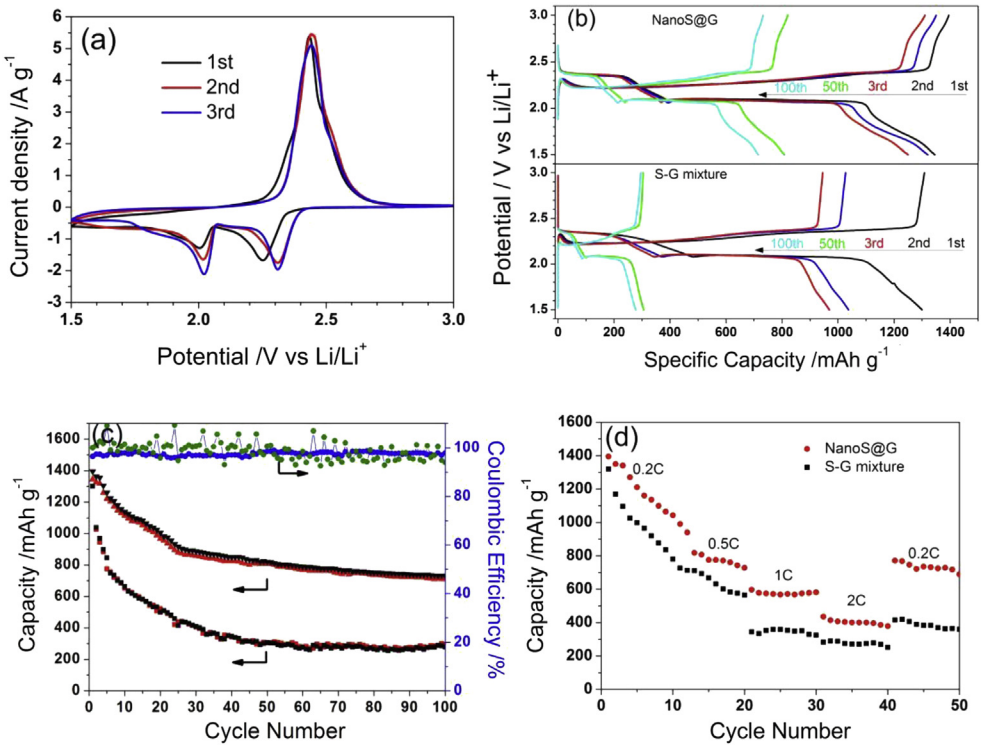

Fig. 7. (a) Cyclic voltammograms of the NanoS@G composite at 0.1 mV s^{-1}; (b) galvanostatic discharge/charge profiles of the NanoS@G composite and S–G mixture in the voltage window of 3.0–1.5 V at 0.2C; (c) cycling performance of the NanoS@G composite and the S–G mixture at 0.2C rate; (d) capacity of the NanoS@G composite and S–G mixture at different rates.

Table 2
Electrochemical performance of various sulfur graphene composite materials.

	Sulfur content/ wt%	Current rate/ mA g^{-1}	Initial discharge capacity/ mAh g^{-1}	Utilization of sulfur	Capacity after cycling (cycle number)	Ref.
Graphene/sulfur coated by reduced graphene oxide	63	200	1600	95.7	900 (100)	[11]
Sulfur nanocrystal/fibrous graphene hybrid	63	750	710	42.5	541 (100)	[20]
Sulfur/three-dimensional graphene/MWCNT	70	335	1396	83.5	844 (100)	[22]
Uniformly dispersed sulfur on reduced graphene oxide	49	167	1400	83.7	627 (80)	[23]
Graphene-wrapped sulfur particles	67	335	750	44.8	530 (100)	[24]
Reduced graphene oxide encapsulated sulfur	65	1672	720	43.0	622 (60)	[25]
Sulfur graphene mixture	22	50	1611	96.4	600 (40)	[26]
Sulfur graphene mixture	50	335	1300	77.6	320 (100)	This work
Sulfur anchored graphene	50	335	1400	83.7	720 (100)	This work

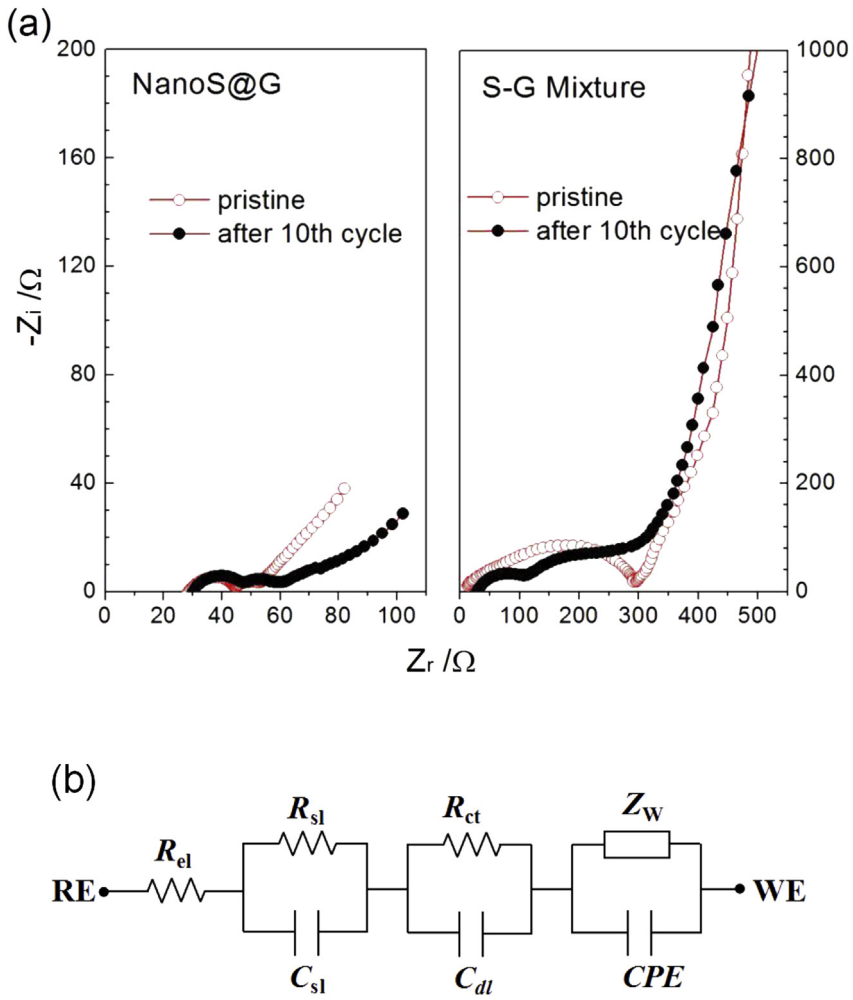

Fig. 8. (a) EIS plots of electrodes with the S–G mixture and the NanoS@G composite; (b) the equivalent circuit used for fitting the experimental data.

polysulfides species and suppressed the "shuttle effect", resulting higher utilization of sulfur, higher coulombic efficiency and better capacity retention. Electrochemical impedance also suggested that the strong bonding enabled rapid electronic/ionic transport and improved electrochemical kinetics, therefore good rate capability was obtained. These results demonstrated that the NanoS@G composite was a very promising candidate for high-performance Li–S batteries.

Table 3
Fitting results of Fig. 8.

Sample		R_{el} (Ω)	R_{sl} (Ω)	R_{ct} (Ω)
NanoS@G	Pristine	22.8	12.3	16.6
	10th cycle	24.4	13.7	14.1
S–G mixture	Pristine	21.9	200.7	71.1
	10th cycle	29.4	260.9	66.1

Acknowledgments

This work was supported by the National Natural Science Foundation of China (NSFC No. 21203168), the Department of Science and Technology of Zhejiang Province (No. 2013C31070), Open Fund of the Key Laboratory of Advanced Materials and Applications for Batteries of Zhejiang Province (No. 2013001), and Zhejiang Xinmiao Talent Program (No. 2013R404073).

References

[1] P.G. Bruce, S.A. Freunberger, L.J. Hardwick, J.M. Tarascon, Nat. Mater. 11 (2012) 19–29.
[2] J. Hassoun, B. Scrosati, Angew. Chem. Int. Ed. 49 (2010) 2371–2374.
[3] M.K. Song, E.J. Cairns, T.G. Zhang, Nanoscale 5 (2013) 2186–2204.
[4] D. Aurbach, E. Pollak, R. Elazari, G. Salitra, C.S. Kelley, J. Affinito, J. Electrochem. Soc. 156 (2009) A694–A702.
[5] G. Zheng, Y. Yang, J.J. Cha, S.S. Hong, Y. Cui, Nano Lett. 11 (2011) 4462–4467.
[6] S. Doerfler, M. Hagen, H. Althues, J. Tuebke, S. Kaskel, M.J. Hoffmann, Chem. Commun. 48 (2012) 4097–4099.
[7] X.L. Ji, K.T. Lee, L.F. Nazar, Nat. Mater. 8 (2009) 500–506.
[8] J. Zhang, J.Y. Xiang, Z.M. Dong, Y. Liu, Y.S. Wu, C.M. Xu, G.H. Du, Electrochim. Acta 116 (2014) 146–151.
[9] B. Ding, C. Yuan, L. Shen, G. Xu, P. Nie, Q. Lai, X. Zhang, J. Mater. Chem. A 1 (2013) 1096–1101.
[10] S. Evers, L.F. Nazar, Chem. Commun. 48 (2012) 1233–1235.
[11] N. Li, M. Zheng, H. Lu, Z. Hu, C. Shen, X. Chang, G. Ji, J. Cao, Y. Shi, Chem. Commun. 48 (2012) 4106–4108.
[12] G.M. Zhou, S.F. Pei, L. Li, D.W. Wang, S.G. Wang, K. Huang, L.C. Yin, F. Li, H.M. Cheng, Adv. Mater. 26 (2014) 625–631.
[13] X.Y. Zhao, J.P. Tu, Y. Lu, J.B. Cai, Y.J. Zhang, X.L. Wang, C.D. Gu, Electrochim. Acta 113 (2013) 256–262.
[14] L.F. Xiao, Y.L. Cao, J. Xiao, B. Schwenzer, M.H. Engelhard, L.V. Saraf, Z.M. Nie, G.J. Exarhos, J. Liu, Adv. Mater. 24 (2012) 1176–1181.
[15] W.D. Zhou, Y.C. Yu, H. Chen, F.J. DiSalvo, H.D. Abruna, J. Am. Chem. Soc. 135 (2013) 16736–16743.
[16] Y. Fu, Y.S. Su, A. Manthiram, J. Electrochem. Soc. 159 (2012) A1420–A1424.
[17] Z.M. Dong, J. Zhang, X.Y. Zhao, J.P. Tu, Q.M. Su, G.H. Du, RSC Adv. 3 (2013) 24914–24917.
[18] L.W. Ji, M.M. Rao, H.M. Zheng, L. Zhang, Y.C. Li, W.H. Duan, J.H. Guo, E.J. Cairns, Y.G. Zhang, J. Am. Chem. Soc. 133 (2011) 18522–18525.
[19] L. Zhou, X.J. Lin, T. Huang, A.S. Yu, J. Mater. Chem. A 2 (2014) 5117–5123.
[20] Y. Zhou, Q. Bao, L.A.L. Tang, Y. Zhong, K.P. Loh, Chem. Mater. 21 (2009) 2950–2956.
[21] C. Nethravathi, M. Rajamathi, Carbon 46 (2008) 1994–1998.
[22] Z. Liu, J. Tang, C.Y. Kang, C.W. Zou, W.S. Yan, P.S. Xu, Solid State Commun. 11 (2012) 960–963.
[23] G.M. Zhou, L.C. Yin, D.W. Wang, L. Li, S.F. Pei, I.R. Gentle, F. Li, H.M. Cheng, ACS Nano 7 (2013) 5367–5375.
[24] R.S.C. Smart, W.M. Skinner, A.R. Gerson, Surf. Interface Anal. 28 (1999) 101–105.
[25] R.J. Chen, T. Zhao, J. Lu, F. Wu, L. Li, J.Z. Chen, G.Q. Tan, Y.S. Ye, K. Amine, Nano Lett. 13 (2013) 4642–4649.
[26] H. Sun, G.L. Xu, Y.F. Xu, S.G. Sun, X.F. Zhang, Y.C. Qiu, S.H. Yang, Nano Res. 5 (2012) 726–738.
[27] H. Wang, Y. Yang, Y. Liang, J.T. Robinson, Y. Li, A. Jackson, Y. Cui, H. Dai, Nano Lett. 11 (2011) 2644–2647.
[28] F.F. Zhang, X.B. Zhang, Y.H. Dong, L.M. Wang, J. Mater. Chem. 12 (2012) 11452–11454.
[29] J.Z. Wang, L. Liu, M. Choucair, J.A. Stride, X. Xu, H.K. Liu, J. Power Sources 196 (2011) 7030–7034.